Cement & Concrete Composites 37 (2013) 143–153

Contents lists available at SciVerse ScienceDirect

Cement & Concrete Composites

journal homepage: www.elsevier.com/locate/cemconcomp

How does fly ash mitigate alkali–silica reaction (ASR) in accelerated mortar bar test (ASTM C1567)?

Seyed M.H. Shafaatian [a], Alireza Akhavan [b], Hamed Maraghechi [b], Farshad Rajabipour [c,*]

[a] I.S. Engineers, 245 Commerce Green Boulevard, Suit #200, Sugar Land, Texas 77478, USA
[b] The Pennsylvania State University, 3127 Research Drive, State College, PA 16801, USA
[c] The Pennsylvania State University, 223B Sackett Building, University Park, PA 16802, USA

ARTICLE INFO

Article history:
Received 10 May 2012
Received in revised form 7 November 2012
Accepted 10 November 2012
Available online 27 November 2012

Keywords:
Alkali–silica reaction
Fly ash
Pore solution
Glass
Diffusion

ABSTRACT

ASTM C1567 [1] is a commonly used accelerated test method to determine the required dosage of supplementary cementitious materials (SCMs) to mitigate alkali–silica reaction (ASR) in mixtures containing reactive siliceous aggregates. Past research suggested that fly ash and other SCMs inhibit ASR, primarily through alkali dilution and binding. In ASTM C1567, however, the alkalinity of the pore solution is largely influenced by the penetration of NaOH from the external soak solution; and this could erase the beneficial effects of alkali dilution and binding. To better understand why fly ash inhibits ASR in this test, the present study performs a quantitative evaluation of six potential ASR mitigation mechanisms: (1) alkali dilution, (2) alkali binding, (3) mass transport reduction, (4) increasing tensile strength, (5) altering ASR gel, and (6) reducing aggregate dissolution rate. The results suggest that (2), (3), (4), and (6) are the primary mitigation mechanisms, while (1) and (5) show a negligible impact.

1. Introduction

Alkali–silica reaction (ASR) is a deleterious reaction in which metastable silicates contained in many natural aggregates dissolve in the highly alkaline pore solution of concrete and further coagulate to form a colloidal alkali–lime–silica gel [2,3]. This gel is hygroscopic and could swell considerably by imbibing moisture [4]. The resulting tensile stresses can lead to cracking and deterioration of concrete [5]. It has been shown that fly ash and other supplementary cementitious materials (SCMs) can be effective in mitigating ASR damage [6–10], and different mechanisms have been proposed to explain how SCMs may control ASR in field and laboratory conditions [11–15]. For example, past research using concrete outdoor exposure blocks and the long-term prism expansion tests (ASTM C1293 [16]) have suggested that SCMs mitigate ASR, among other effects, through reduction of concrete pore solution alkalinity by alkali dilution and binding [10,17,18]. On the other hand, little quantitative information is available to determine the most dominant ASR mitigation mechanisms during the accelerated mortar bar test (ASTM C1567 [1]). In this test, specimens are submerged inside a highly alkaline bath (1 M NaOH) at a high temperature (80 °C). As such, the kinetics of ASR may be dominated by the rate of ion transport inside the mortar as opposed to the ability of SCM in diluting and binding the pore solution alkalis.

The goal of this paper is to use a combined experimental and computer simulation approach to quantitatively determine the contributions of different mechanisms that lead to ASR mitigation by fly ash during the ASTM C1567 test. Crushed soda–lime–silica glass is used as reactive aggregates in preparation of neat Portland cement and cement-fly ash mortars. A variety of analytical tools are used to study the mortar microstructure, its mechanical and transport properties, pore solution composition, aggregate dissolution rate, and ASR gel formation and composition.

Due to its simplicity and time effectiveness, the accelerated mortar bar test is widely used in specifications and QC/QA applications to assess the potential reactivity of an aggregate source or the ASR performance of combinations of SCMs and aggregates [19,20]. The authors acknowledge that, by exposing aggregates to an excessively harsh environment, this test is considered less reliable than the outdoor exposure of concrete blocks [21] or the concrete prism expansion test (ASTM C1293) [22,23]. However, given that this standard test is widely used and has been adopted by many construction specifications, it is important to better understand the reaction mechanisms in this test and to determine exactly what underlying mechanisms result in mitigation of ASR when SCMs are used in combination with reactive aggregates.

2. Existing literature

Prior studies have identified seven potential mechanisms for mitigation of ASR by fly ash: alkali dilution, alkali binding, limiting

* Corresponding author. Tel.: +1 814 863 0601; fax: +1 814 863 7304.
E-mail address: farshad@psu.edu (F. Rajabipour).

0958-9465/$ - see front matter © 2012 Elsevier Ltd. All rights reserved.
http://dx.doi.org/10.1016/j.cemconcomp.2012.11.004

mass transport, improving strength, modifying ASR gel, consumption of portlandite, and supplying soluble alumina. A brief description of each mechanism is provided below.

(1) Alkali dilution: the alkalinity of concrete's pore solution is reduced by replacing cement with fly ash [11,13]. Even when the Na_2O_{eq} content of fly ash is higher than cement's, the dilution effect is observed as only a portion of fly ash alkalis are soluble per ASTM C311 test [4,24]; and even that portion dissolves slowly in the pore solution due to slower reactivity of fly ash in comparison with Portland cement [11].
(2) Alkali binding: the additional pozzolanic C–S–H is able to bind alkali and hydroxyl ions and remove them from the pore solution [25,26]. In addition to increasing the volume fraction of C–S–H, the pozzolanic C–S–H has a lower C/S, and shows a higher alkali binding capacity in comparison with C–S–H from cement hydration [10,27]. This may be attributed to increasing the acidity of silanol (Si–OH) groups [28] or developing alkali attractive (i.e., negative) surface charges on the low C/S C–S–H [29]. Based on the results of ASTM C1293 test [16], it has been shown that pore solution alkalinity of concrete is strongly correlated with the ASR prism expansions [30]. Fly ashes with high Na_2O_{eq} and CaO contents have been found to be less efficient in reducing pore solution alkalinity, and also less effective in controlling ASR [26,31].
(3) Limiting mass transport: pozzolanic reactions can, over time, reduce the mass transport properties of concrete [32]. A reduction in the ion diffusion coefficient is significant especially where an external source of alkalis is present. In addition, a reduction in the hydraulic permeability of concrete can slow down the absorption of water and swelling of the ASR gel [41]. Despite the importance of mass transport for long-term measurements, the significance of this mechanism for accelerated tests is unclear. Fly ash generally reacts slower than Portland cement and it has been reported that concrete containing fly ash generally has higher porosity and transport properties at early-ages in comparison with 100% Portland cement concrete [33,34].
(4) Improving tensile strength: fly ash concrete, over time, develops a higher tensile strength which aids in resisting internal stresses and cracking [35]. Again, it is unclear whether the tensile strength is improved or reduced at early ages due to slow reactivity of fly ash.
(5) Modifying ASR gel properties: by changing the composition of ASR gel, fly ash may reduce the swelling capacity, swelling pressure, and viscosity of ASR gel. Monteiro et al. [29] observed that high CaO/Na_2O_{eq} gels have lower swelling capacity than gels with low CaO/Na_2O_{eq}. Struble and Diamond [36] reported that calcium-free sodium-silicate gels can become fluid (i.e., lose their viscosity) under moderate pressures; unlike calcium-rich gels which remain solid. Similarly, Bleszynski and Thomas [37] observed that very low CaO/Na_2O_{eq} gels can diffuse freely into surrounding cement paste without exerting damage; which may indicate their low viscosity and swelling pressure. Bonakdar et al. [38] related the composition of ASR gel to the number of bridging oxygens in the silica tetrahedra, and reported that gels produced in a less basic environment (e.g., fly ash) have a fibrous structure, which results in limited swelling pressure, comparing with the 3-dimensional gels formed without fly ash.
(6) Consumption of portlandite: it has been suggested that the presence of $Ca(OH)_2$, or other soluble sources of Ca, is necessary for formation of expansive ASR gel [37,39,40]. As a result, consumption of portlandite by the pozzolanic reaction may reduce the tensile stresses resulting from formation and swelling of the ASR gel [41]. Portlandite can also serve as a pH buffer to maintain the pore solution's pH above 12.6. However, the pH of pore solution is generally larger than 13.0 due to the presence of alkali sulfates in Portland cement [42].
(7) Supplying soluble alumina: Al-rich SCMs (e.g., fly ash, metakaolin) have been found to be more effective against ASR than SCMs with higher silica purity (e.g., silica fume) [8,43,44]. The alumina in fly ash can dissolve into pore solution and be further incorporated into the pozzolanic reactions to form C–A–S–H (also known as Al-modified C–S–H) gel. Hong and Glasser [45] suggested that presence of Al in C–S–H can considerably enhance its alkali binding capacity. On the other hand, Chappex and Scrivener [46] reported that alumina contributed by SCMs did not reduce the alkalinity of paste pore solutions. In addition, presence of Al in pore solution may reduce the dissolution rate of silica [47,48], possibly due to adsorption of Al at silica surfaces or the formation of a protective alumino-silicate layer [49,50].

In this paper, the first five mechanisms from the above list are investigated. Parallel studies are in progress, and will be reported in future publications, to better characterize the role of portlandite and alumina in the reactions. Additionally in this paper, a new mechanism that could contribute to mitigation of ASR is proposed and evaluated in Section 5.7. It is hypothesized that the presence of fly ash can reduce the dissolution rate of siliceous aggregates even where no pH reduction can be achieved (e.g., near the surface of ASTM C1567 mortar bars where the pH of the pore solution is controlled by the external alkali bath). In other words, even without reducing the alkalinity of pore solution, fly ash (and possibly other SCMs) could be capable of reducing the aggregate dissolution rate. As discussed in Section 5.7, this may be linked to a large surface area of amorphous silicates provided by fly ash, which attracts OH^- ions and reduce their effective concentration at the surface of reactive aggregates, effectively producing a local reduction in pH.

Given that recycled soda–lime–silica glass (e.g., crushed container or window glass) is used as reactive aggregates in this study, a brief literature review on the alkali–silica reactivity of this material is useful. Soda–lime glass contains a homogenous matrix of highly amorphous silicate. The typical chemical composition includes SiO_2 (>70%), Na_2O (~13%), and CaO (~11%). Since glass particles are crushed, they are angular and have residual intra-particle microcracks. ASR induced by recycled glass aggregates shows a considerable size effect in which larger glass particles are more reactive than smaller particles [51]. This trend is counter intuitive as increasing the particle surface area should accelerate the reactions; assuming that ASR occurs at the glass–cement paste interface. SEM examination of ASTM C1293 and C1260 [52] specimens affected by ASR revealed that glass particles do not undergo ASR at their surface [51,53]. Rather, ASR initiates inside intra-particle cracks which are originated during bottle crushing (i.e., they exist before glass is mixed in concrete). Larger particles contain wider cracks and a higher crack density which result in a higher alkali silica reactivity [53]. The hypothesis that residual bottle crushing cracks are responsible for ASR was validated by two further observations. First, soda–lime glass beads with the same oxide composition but no internal cracks were found to be innocuous when tested by ASTM C1260 [54]. Second, annealing of crushed glass cullet to heal the residual cracks was found to mitigate ASR [53]. The reason that the glass–paste interface is protected from ASR is not clearly understood, but may be related to deposition of portlandite (CH) which favors a pozzolanic reaction [55]. Evidence of a pozzolanic reaction and C–S–H formation at the interface has been observed using SEM/EDS [51].

3. Materials and methods

Mortar mixtures were prepared according to the proportions of ASTM C1567 [1] using pulverized recycled soda–lime glass sand and a mixture of Portland cement and fly ash as binder. ASTM C150 [56] type I Portland cement was used. Six ASTM C618 [57] fly ashes were studied including four class F (identified as F1, F2, F3, F4), and two class C (identified as C1, C2). Fly ashes were used at different cement replacement levels (mass based) to evaluate their efficiency in controlling ASR. A control mortar containing 100% Portland cement was also tested. The oxide composition of cement, glass, and all fly ashes are presented in Table 1, along with their specific gravity and median particle size. Recycled glass sand was composed of three main colors: amber (~30%), clear (~30%) and green (~40%). Glass bottles were washed and crushed using a ball mill. All mortars were prepared with water-to-cementitious materials ratio (w/cm) = 0.47, and a 53% volume fraction of sand with gradation in the range of 4.75 mm–150 μm according to ASTM C1567 [1]. Mortars were mixed according to ASTM C305 [58]. Specimens were prepared and moist cured for 24 h at 23 °C. After 24 h, specimens were demolded and cured submerged in water at 80 °C for another 24 h. Finally, the specimens were transferred to a 1 M NaOH bath at 80 °C and maintained for 14 days. The following tests were performed on the mortars.

3.1. Accelerated mortar bar test (ASTM C1567)

This test was used to determine the dosage of each type of fly ash needed to reduce the mortar bar expansion below the innocuous threshold of 0.1%. A total of 56 different mixtures were tested. For each mixture, four 25 × 25 × 250 mm prisms were prepared with embedded gage studs at the ends to facilitate length measurements. A digital comparator with an accuracy of 0.0025 mm was used. Prism lengths were measured after demolding, 24 h of water curing, and 1, 3, 5, 7, 10, and 14 days submersion in the NaOH bath.

3.2. Pore solution extraction and analysis

To investigate the impact of fly ash on pore solution ion concentrations, and to quantify the extent of alkali dilution, binding, and transport, pore solution of the control (100%PC), 15%F1 and 35%C2 mortars were extracted. The latter two mortars contained sufficient fly ash to suppress ASR expansions below 0.1%. Pore solution extraction was performed immediately after mixing, after demolding (24 h), and at 0, 3, 7, and 14 days of NaOH bath exposure. Pore solution of plastic mortar was extracted by pressure filtration using nitrogen gas. For hardened samples, mortar prisms were removed from the baths, surface dried, broken into smaller pieces, and then pressurized inside a pore solution extraction die up to a maximum stress of 550 MPa at a controlled rate of 75 MPa/min. The extracted solutions were collected in sealable PP vials, filtered through 0.2 μm PTFE membrane filters, and immediately tested by HCl titration to measure [OH^-]. The concentrations of other elements (Na, K, Ca, Si, Al and S) were measured using a Perkin–Elmer Optima 5300 ICP-AES.

3.3. Measurement of ion diffusivity using electrical impedance spectroscopy

The ion diffusion coefficient of mortars (D, m^2/s) was determined using non-destructive electrical conductivity measurements according to the Nernst–Einstein equation [59,60]:

$$D = D_o \frac{\sigma}{\sigma_o} \quad (1)$$

where σ (S/m) is the electrical conductivity of mortar, σ_o (S/m) is the conductivity of pore solution, and D_o (m^2/s) is the diffusion coefficient of ions in pore solution. For information on the scientific basis of this method and details of measurements and data interpretation, please see [60,61]. Samples from three mortars were tested: control, 15%F1, and 35%C2. The electrical conductivity of the mortars (σ) was measured between a pair of 3.2 mm-diameter stainless steel electrodes embedded through the thickness of each mortar bar with a 15 mm distance between the centers of the electrodes. The bulk resistance was measured using an HP-4194A impedance analyzer in frequency sweep mode (40 Hz–10 MHz) and using 250 mV voltage. The results were converted to electrical conductivity using an experimentally established geometry factor [62]. The measurements were performed after 0, 3, 7, and 14 days of mortars exposure to NaOH bath. An average of four measurements, obtained from four duplicate specimens, was used to establish each data point. In parallel, pore fluids of mortars were extracted (as described above) and their electrical conductivity (σ_o) was measured using a commercial conductivity probe. The value of ion diffusivity in pore solution was not physically measured but assumed as $D_o = 1.065 \times 10^{-9}$ m^2/s for NaOH in water at 80 °C [63]. This value corresponds to the effective self-diffusion coefficient of NaOH that is calculated according to the formula by [63] using the diffusivity of Na^+ and OH^- ions. The self-diffusion coefficient does not consider the reduced ion activity due to ion–ion interactions at high concentrations. However, given that the ionic strength of the control, 15%F1, and 35%C2 are comparable (Fig. 2),

Table 1
Oxide composition (wt.%) and physical properties of Portland cement, glass, and fly ashes.

Oxide	Cement	Glass	F1	F2	F3	F4	C1	C2
CaO	62.50	10.62	2.42	1.26	3.81	13.52	26.63	27.33
SiO_2	19.90	73.13	51.75	59.93	49.20	52.23	33.48	34.02
Al_2O_3	5.44	1.99	33.70	24.97	23.34	16.36	18.59	18.74
Fe_2O_3	2.26	0.52	4.08	6.33	14.72	5.78	6.13	5.86
Na_2O	0.30	13.74	0.40	0.36	0.69	2.82	0.37	1.50
K_2O	0.89	0.34	1.16	1.90	1.78	2.16	0.72	0.35
MgO	2.31	0.53	0.60	1.00	1.03	4.30	1.48	5.00
MnO	0.09	N/D[a]	0.03	0.07	0.03	0.05	0.03	0.05
TiO_2	0.29	N/D[a]	1.30	1.48	1.03	0.64	1.95	1.57
SO_3	4.93	N/D[a]	0.25	1.33	1.47	1.17	7.65	3.67
P_2O_5	0.23	N/D[a]	0.30	0.28	0.35	0.18	0.26	1.03
LOI	0.86	–	4.01	1.09	2.55	0.80	2.71	0.88
C/S	3.14	0.19	0.05	0.02	0.08	0.26	0.80	0.80
Na_2O_{eq}	0.89	13.96	1.16	1.61	1.86	4.24	0.84	1.73
Specific gravity	3.14	2.46	2.24	2.44	2.46	2.44	2.69	2.66
Med particle size (μm)	14.1	–	13.8	9.9	19.1	13.6	22.5	8.6

[a] N/D is not detected.

it is acceptable to assume that the effect of ion activity on D_o of the three pore solutions is approximately similar.

3.4. Tensile and compressive strength tests

To examine the effect of fly ash on the tensile strength (i.e., modulus of rupture) of mortars, $25 \times 25 \times 250$ mm prisms were tested in 3-point bending. Specimens were prepared according to ASTM C1567 and using a dosage of each fly ash that controlled expansions to below 0.1%: 15%F1, 15%F2, 20%F3, 20%F4, 25%C1 and 35%C2. The specimens were prepared and cured following the procedure of ASTM C1567: the specimens were demolded at 24 h, cured under water for 24 h at 80 °C and then transferred to a 1 M NaOH bath. The prisms were tested after 3 days soaking in the NaOH bath at 80 °C. ASTM C1567 measurements showed macroscopic expansions starting in the control (100%PC) mortar after 3 days NaOH exposure. As such, this time was chosen as the onset of macro-cracking. Prisms were tested using a displacement-controlled setup that applied a mid-span deformation of 5 μm/s until failure. The compressive strength of similarly cured mortar cubes ($50 \times 50 \times 50$ mm) was tested according to ASTM C109. For both tensile and compressive strength tests, an average of three measurements was used per each mixture.

3.5. SEM/EDS imaging

SEM/EDS imaging was used to study the microstructure of the mortars, and to study ASR gel formation and composition. Imaging was performed on the control, 15%F1, and 35%C2 mortars. After 7 and 14 days of NaOH exposure, cross sections were saw-cut from mortar bars with an approximate thickness of 1 cm. Specimens were vacuum dried inside a desiccator for 48 h and then impregnated with a low viscosity epoxy. After setting, the surface epoxy was polished off and the specimens were successively polished with 30, 15, 9, 6, 3 and 1 μm grits. Polishing oil was used instead of water to prevent leaching. Specimens were carbon coated prior to SEM. Image acquisition was performed in the BSE mode using an FEI Quanta 200 ESEM instrument with a lateral resolution of 3.5 nm. The ESEM was equipped with an X-ray energy dispersive spectroscopy (EDS) detector for compositional analysis. EDS spot analysis was performed on at least 20 ASR gel points for the control, 15%F1 and 35%C2 mortar cross sections to gain information regarding the composition of ASR gels. The gel composition was examined after 7 and 14 days of NaOH exposure to monitor changes in its composition over time.

3.6. Aggregate dissolution rate measurements

To assess the dissolution rate of glass aggregates in the presence or absence of fly ash, a glass corrosion experiment was performed. Soda–lime glass slides ($75 \times 25 \times 1$ mm) were submerged in 340 ml of 1 M NaOH solution at 80 °C for a period of 14 days. Solutions were not stirred during the experiments. Periodic mass loss measurements from glass slides were used to monitor the dissolution rate of glass. For each measurement, the glass slides were removed from the solution and the silica gel formed on the surface of each slide was carefully washed off by deionized water. Mass measurements were performed using a balance with accuracy of 0.0001 g. For each data point, measurements were obtained from two duplicate slides. The corrosion experiments were performed in the absence of fly ash, and also for systems where 10 g or 20 g of F1 fly ash was added to the solution. The corrosion tests were performed inside sealable plastic containers to minimize evaporation and carbonation. The [OH^-] was periodically monitored by sampling the solution and performing acid titration.

4. Numerical model to simulate alkali transport and binding

A numerical model was developed to assess the simultaneous effects of ion diffusion and binding on the pore fluid concentration of mortars during the ASTM C1567 test. Several simplifying assumptions were made during development of this model, as described below. As such, the results only provide a semi-quantitative evaluation of the relative significance of ion diffusion and binding, and should not be directly compared with pore fluid compositions of mortars that were measured experimentally (Section 5.2).

A 1D finite-difference model was developed to simulate the diffusion of NaOH from the soak solution by solving the Fick's 2nd law. The alkali binding effect was accounted for by introducing a sink term in the model. Ion diffusion was simulated within a mortar cross section of 25×25 mm^2 that was exposed to 1 M NaOH from two opposite faces (Fig. 4). The other two faces were sealed (1D model). Mortar diffusion coefficients were obtained experimentally (Section 5.3) at the time of submerging samples into the NaOH bath (i.e., 2 days after casting). For the 100%PC mortar, $D = 1.16 \times 10^{-11}$ m^2/s and for the 15%F1 mortar, $D = 3.02 \times 10^{-12}$ m^2/s was used. Diffusion coefficients were assumed to remain constant during the simulations. Diffusivity of NaOH in pore solution (D_o) at 80 °C was used as 1.065×10^{-9} m^2/s [63], without considering the effect of ion activity coefficients. The model included a sink term to account for alkali binding by C–S–H according to the distribution ratio R_d [28]:

$$R_d = \frac{[\text{Na}] \text{ in solid C—S—H (Mol/kg)}}{[\text{Na}] \text{ in pore solution (Mol/kg)}} \quad (2)$$

Based on the work of Hong and Glasser [28], the equilibrium distribution ration (R_d) is a function of the Ca/Si of the C–S–H. For 100%PC mortar (Ca/Si = 1.87), $R_d = 0.5$; and for 15%F1 mortar (Ca/Si = 1.39), $R_d = 1.25$ were used. This suggests a better binding capacity for mortars containing fly ash. The Ca/Si was determined by EDS of the C–S–H phase in the 100%PC and 15%F1 mortars. At least 20 EDS spot analyses were performed on C–S–H rims around cement and fly ash particles, and the average Ca/Si was obtained. The mass fraction of C–S–H was assumed to be the same for both 100%PC and 15%F1 pastes ($m_{C\text{–}S\text{–}H} \approx 50$ wt.% of each paste, based on results of [64,65] for neat cement pastes and cement-fly ash pastes). At every time step ($\Delta t = 15$ min), [Na] in pore solution was calculated based on the Fick's law. Subsequently, [Na] in pore solution was adjusted by subtracting the amount that can be absorbed by the solid phase according to Eq. (2). The model then proceeded to the next time step and the simulation continued. An inherent assumption in the model is that chemical equilibrium between the solutes and C–S–H is achieved within each time step ($\Delta t = 15$ min).

The pore solution was assumed to only contain Na and OH ions; as such multi-ion diffusion was ignored. At every point within the pore solution, charge neutrality was maintained meaning: [Na^+] = [OH^-]. The initial condition was defined as [OH^-] = 0.23 M across the thickness of the mortar for both control and fly ash mortars. This value reflects the [OH^-] for the control mortar at 48 h after casting and before exposure to NaOH (Fig. 2a). The 15%F1 mortar showed smaller [OH^-] at this time; however the same value of [OH^-] = 0.23 M was chosen in the simulation of both mortars so the final results exclusively represent the contribution of NaOH diffusion and binding during the 14-day bath exposure period. Further OH^- release due to continued hydration of cement and fly ash beyond 48 h was assumed negligible. The model's boundary condition was [OH^-] = 1.0 M at 0 and 25 mm (i.e., the bath concentration).

5. Results and discussion

5.1. Sufficient dosage of fly ash to mitigate ASR

The average expansion of all mortar mixtures at the conclusion of the ASTM C1567 test (i.e., 14 days NaOH exposure) is presented in Table 2. Based on these results, all fly ashes can mitigate ASR but at different dosage levels. The minimum cement replacement levels to achieve expansions below 0.1% were as follows: 15%F1, 15%F2, 20%F3, 20%F4, 25%C1 and 35%C2. A comparison suggests that fly ashes with higher CaO content are less effective in mitigating ASR. This agrees with the existing literature [7,10,26,66] on mitigation of ASR induced by natural aggregates, and could be due to inefficiency of such ashes in maintaining a low alkalinity of pore fluid due to higher penetrability of the matrix or lower alkali binding capacity of the matrix.

Fig. 1 shows the expansion of the control, 15%F1 and 35%C2 mortars during the entire period of the ASTM C1567 test. Expansions in all three mortars were small for the first 3 days exposure to NaOH. Afterwards, while the expansions in fly ash mortars increased slowly for the remainder of the test, the control mortar showed a drastic increase in expansion at 5 days and beyond. The rate of expansion increased after 3 days and remained relatively constant after 5 days. This may suggest that it took ~3 days for the concentration of OH^- ions to build up to sufficient levels in the control mortar to initiate ASR (see Fig. 2a). Comparison with pore solution analysis data suggests that after 5 days, the rate of expansion may not be directly related to $[OH^-]$. This may further imply that ASR kinetics is no longer controlled by the rate of OH^- diffusion, but by the rate of ASR gel formation and swelling.

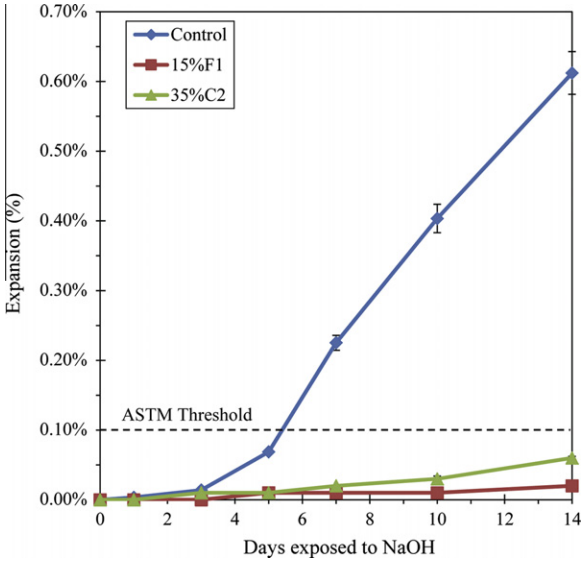

Fig. 1. ASR expansion of control, 15%F1 and 35%C2 mortars during the ASTM C1567.

5.2. Pore solution composition

The results of pore solution analysis are presented in Fig. 2a–e. Fig. 2a shows $[OH^-]$ over the duration of the ASTM C1567 test. At 0 day, all three mortars have $[OH^-] \approx 100$ mM; despite higher Na_2O_{eq} of both fly ashes compared with PC. It should be noted that fly ash alkalis may dissolve slower than cement's due to slow reactivity of fly ash. During the first 24 h, concentrations rise mainly due to cement hydration. At 24 h, $[OH^-]$ of fly ash mortars is 22% and 34% less than the control mortar; which shows the effect of alkali dilution (more dilution for 35%C2 which contains less cement). During the next 24 h, mortars are submerged in a water bath at 80 °C which promotes leaching of alkalis. The rate of leaching is proportional to the ion diffusivity of mortars and is the highest for 100%PC. At 48 h, the $[OH^-]$ has dropped to 170–270 mM and the effect of alkali dilution is erased. The mortar 35%C2 shows the highest $[OH^-]$ despite having the lowest cement content. During the next 14 days, $[OH^-]$ of mortar pore solutions increase steadily due to exposure to the NaOH bath. The control mortar shows the highest rise in concentrations which agrees with its high ion diffusion coefficient (Section 5.3). As both the dissolution rate of glass aggregates and the solubility of silica are strongly related to the pH [47], the highest rate of ASR is observed in the 100%PC mortar. At the test's conclusion, the $[OH^-]$ in the control mortar reaches and surpasses the OH^- concentration of the soak solution (1 M). This is due to an ion exchange mechanism, where alkalis contained in the soda–lime glass or the silica gel are released into the pore solution, resulting in the hydrolysis of water, and an increase in the pore solution's pH [67]:

$$(\equiv Si{-}O{-}Na) + H_2O \leftrightarrow (\equiv Si{-}OH) + (Na^+) + (OH^-) \quad (3)$$

This is further discussed in Section 5.7. Fig. 2b shows variations in elemental [Na] in the pore solution of the three mortars. It must be noted that unlike acid titration, which measures the concentration of OH^- ions, ICP measures the total [Na], which is not the same as ionic $[Na^+]$. As such, there is a chance that small quantities of non-ionic Na may be present in the filtered pore solutions if they are integrated into fine silica gel particles that may have passed the 0.2 μm filter. The same is true for [K], [Ca] and [S]. As a result, it would not be surprising if $\Delta = ([OH^-] + 2[SO_4]) - ([Na]+[K]+2[Ca])$ deviates from zero. In the results reported in Fig. 2a–e, Δ is in the range of ±150 mM. Some of this deviation is also attributed to the variability of experimental results. It should be also mentioned that the pore solution analysis data presented here provide an average composition of the pore solution within each sample. It is acknowledged that concentration gradients exist inside the samples and the pore solutions may not be in full chemical equilibrium with the solid phases inside the sample at the time of extraction. More discussions on the reliability of these measurements are provided in [74].

Table 2
Expansion of mortar mixtures at the conclusion of ASTM C1567 test.

Cement replacement level (%)	Fly ash					
	F1 (%)	F2 (%)	F3 (%)	F4 (%)	C1 (%)	C2 (%)
0	0.60	0.60	0.60	0.60	0.60	0.60
10	0.19					
15	0.02	0.06	0.11	0.15		
20	0.01	0.03	0.03	0.04	0.12	0.26
25		0.01		0.01	0.03	
30	0.00			0.00	0.02	0.09
35						0.06

Highlights represent dosage of each fly ash that resulted in expansion well below the 0.1% threshold.

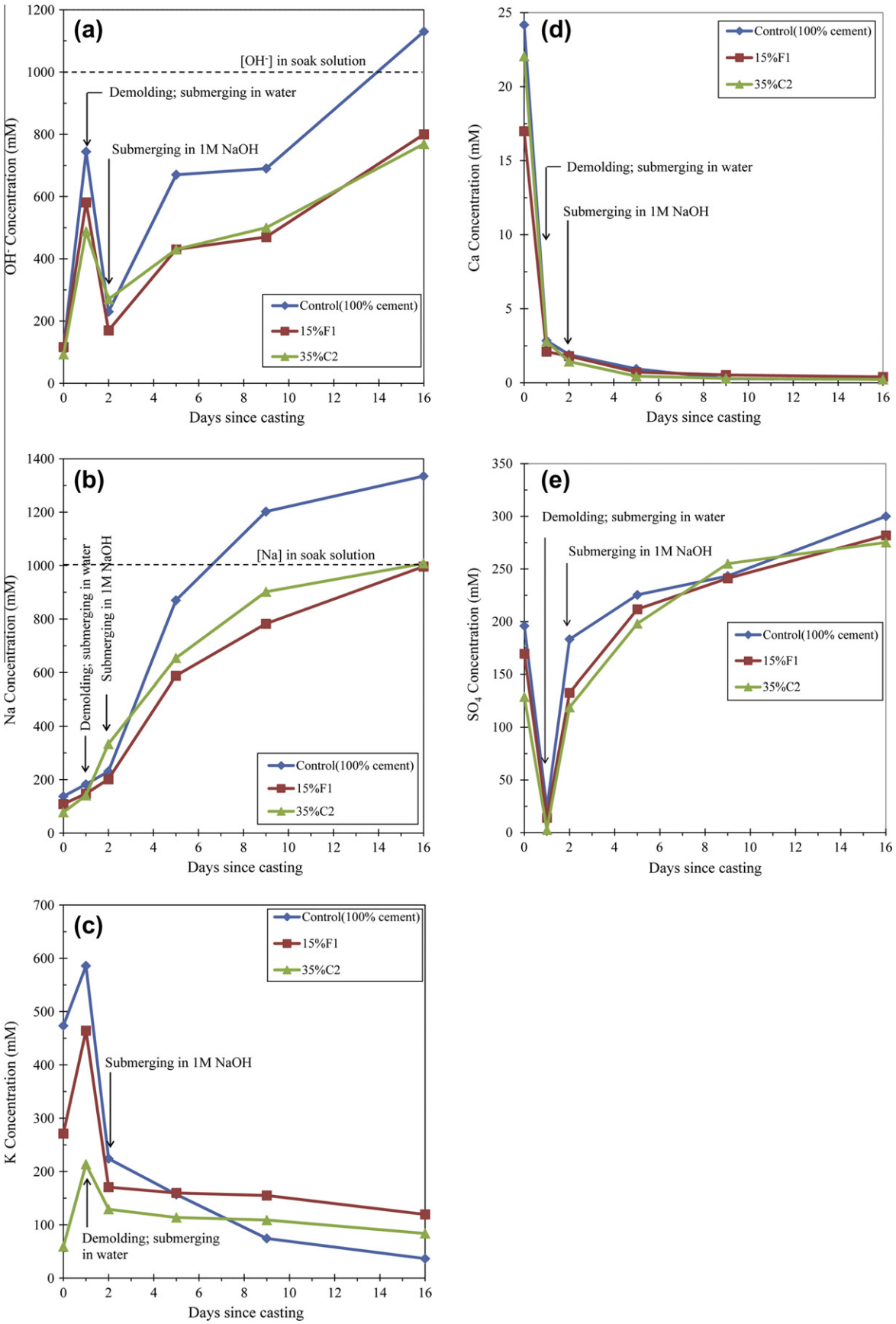

Fig. 2. Pore solution composition of mortars during the ASTM C1567 test: (a) [OH^-], (b) [Na], (c) [K], (d) [Ca], and (e) [SO_4].

Immediately after mixing, [Na] is in the range 78–138 mM, with the 100%PC mortar showing the highest concentration. During the first 48 h, [Na] in all three mortars increases steadily due to reaction of cement and of fly ash. At 48 h, [Na] in 35%C2 mortar is 333 mM in comparison with 231 mM for the control and 202 mM for the 15%F1 mortars. This is likely due to a significantly higher Na_2O content of the C2 fly ash (see Table 1). Interestingly, the water curing period (between 24 and 48 h) did not result in a reduction of [Na]; unlike the trend observed for [OH^-] and [K]. After submersion of the mortar prisms inside 1 M NaOH, the Na contents of pore solutions increase by a factor of up to 5.8 times. This increase was more rapid in the 100%PC mortar which agrees well with its higher ion diffusion coefficient as discussed in the next section. It should be noted that Na can be released from the soda–lime glass aggregates, as well.

Fig. 2c and d show the concentrations of K and Ca in the pore solutions of the three mortars. Large differences in the initial [K] is observed due to dilution of the readily soluble potassium in the fly ash systems. Although the K_2O content of F1 fly ash is higher than the PC (1.16% versus 0.89%), the 15%F1 mortar shows 43% less [K] at 0 day, due to a slower reaction and release of alkalis by fly ash. During the first 24 h, [K] increases in all three mortars, due to dissolution from cement and fly ash. During the water curing period (between 24 and 48 h), potassium content drops by leaching out of the mortars. At 48 h, [K] in the 100%PC mortar is 224 mM compared with 171 mM and 129 mM for the 15%F1 and 35%C2 fly ash mortars, and the effect of alkali dilution is largely erased. During the next 14 days, where mortars are submerged in the NaOH bath, potassium leaching continues, albeit at a slower rate. The control mortar shows a faster rate of K leaching, in agreement with its higher ion diffusivity.

Fig. 2d shows that at the time of casting, the [Ca] of pore solutions is near or above the solubility limit of $Ca(OH)_2$ (≈20 mM at pH = 12.5) [68]. Fly ash mortars show lower [Ca], possibly due to cement dilution. During the first 24 h, [Ca] of pore solution drops drastically, which is in agreement with the available literature [68,69]. This is primarily due to reduction in the calcium solubility as the pH increases [70–72], which results in precipitation of solid CH and C–S–H. The calcium content of pore solutions continues to decrease throughout the experiment, partly due to leaching of Ca to the bath, and partly due to reduction in the CH solubility as pH increases. No significant difference is observed in the [Ca] of the pore solution of the three mortars past 1 day.

Finally, Fig. 2e shows the concentration of SO_4 that is calculated based on the measurements of sulfur (S) content of the pore solutions by ICP. It is assumed that all sulfur measured is in the form of SO_4. At the time of mixing, the control mortar shows the highest concentrations of SO_4 in the pore solution, in agreement with its higher cement (gypsum) content. It should be noted that while the SO_3 content of fly ash C2 is considerable, did not translate into high [SO_4] in the pore solution, potentially due to slow reactivity of fly ash or limited solubility of sulfur from fly ash. During the first 24 h of curing, sulfates in the solution are consumed by the hydration of aluminate phases. As the solid gypsum phase is depleted, the [SO_4] in the pore solution drops to near zero [42,68,70]. As soon as the mortars are placed inside a water or NaOH bath at 80 °C, a substantial increase in the [SO_4] of the pore solution is observed. This increase is likely attributed to the decomposition of ettringite to monosulfate that occurs at the elevated temperature as suggested by Shimada and Young [73]. This hypothesis should be evaluated using X-ray diffraction or thermal methods to monitor the depletion of the ettringite phase during ASTM C1567 test. It should be noted that this is the same mechanism that leads to delayed ettringite formation in heat cured concrete.

5.3. Ion diffusion coefficient

The ion diffusion coefficient of mortars was measured using electrical impedance spectroscopy and according to the Nernst–Einstein equation (1). Fig. 3 shows the results for the control, 15%F1, and 35%C2 mortars over the duration of the ASTM C1567 test. The control mortar shows a significantly larger (by a factor of 4–7) ion diffusivity than the two fly ash mortars. This means that NaOH can penetrate much faster through the 100%PC mortar (in agreement with pore fluid analysis data of Fig. 2); which in turn, results in much larger ASR expansions (Fig. 1). The reduction in the ion diffusivity of the fly ash mortars may be related to a reduced porosity and reduced size of capillary pores. Since the density of fly ashes is less than that of Portland cement (Table 1), replacement of cement with fly ash on a mass basis, while keeping the w/cm constant, results in a net reduction of initial porosity. In the present case, the initial paste porosity for the 100%PC mortar can be calculated as 59.6%. For the 15%F1 mortar, the initial paste porosity is 58.2% and for the 35%C2 mortar, the initial paste porosity is 58.1%. In addition to the porosity reduction, F1 and C2 fly ashes have smaller median particle size comparing to Portland cement. As such, their use as a partial cement replacement could result in reducing the initial size of capillary pores. As reported in [74], mercury porosimetry (MIP) measurements performed on these three mortars, 5 days after casting, show that the average pore size decreases from 32 nm for the Portland cement mortar, to 14 nm and 9 nm for the 15%F1 and 35%C2 mortars, respectively. Electrical conductivity measurements performed at the same age show a large increase in the tortuosity of the pore network [74].

These findings strongly support the role of fly ash in reducing ion transport as a major mechanism by which fly ash mitigates ASR during the ASTM C1567 test. It is observed that even at early ages during this test, fly ash mortars show a considerably lower diffusion coefficient. Note that these mortars are water cured for 24 h at 80 °C which can boost the reactivity of fly ash. It is also observed in Fig. 3 that the diffusivity of the control mortar increases from 2 to 5 and 9 days, but subsequently decreases. To make sure that this is not an experimental error, the tests were repeated and similar results were obtained. The initial increase in diffusivity is probably due to microcracking caused by ASR. As these cracks are filled by ASR gel (with much lower electrical conductivity and ion diffusivity than the pore solution); the overall

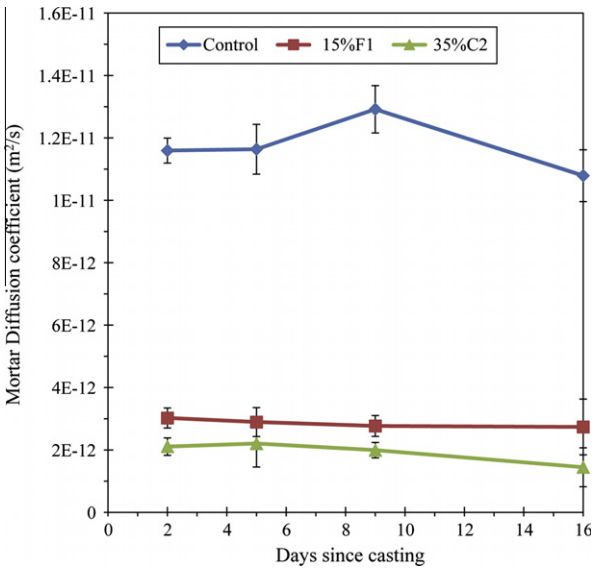

Fig. 3. Ion diffusion coefficient of the control (100% PC), 15%F1 and 35% C2 mortars.

conductivity/diffusivity of the mortar decreases. The diffusivity of the fly ash mortars remained relatively constant during the test period, which implies a low level of microcracking in fly ash mortars.

5.4. Significance of alkali diffusion versus binding

It was observed in Fig. 2a that fly ash mortars have a smaller concentration of OH^- ions in their pore solution; which helps in reducing the ASR. Yet, it is not clear to what extent this reduction in $[OH^-]$ is due to the lower ion diffusivity of mortars versus the mortars' improved alkali binding capacity. The numerical modeling results provided in Fig. 4 are aimed at addressing this question. The figure shows the simulated $[OH^-]$ profiles as a result of the penetration and binding of NaOH during the ASTM C1567 test. Here, the triangles represent the control (100%PC) mortar; where the OH^- front has reached the centerline of the specimen (position = 12.5 mm) within 14 days of NaOH bath exposure. Larger $[OH^-]$ would be anticipated at the specimen's interior had a more realistic 2D model been used, or if the model accounted for the effect of cracking on increasing the mortar diffusion coefficient. SEM imaging confirmed the presence of ASR gel across the control mortar's cross section, but the severity of ASR attack and the volume of gel formed was considerably higher at the specimen's surface.

The squares in Fig. 4 show the simulated $[OH^-]$ profile corresponding to the 15%F1 mortar. This mortar shows lower $[OH^-]$ due to a combination of lower ion diffusivity and higher C–S–H binding capacity. In comparison with the 100%PC mortar, the NaOH penetration depth is limited to approximately 5 mm from the surface; which accounts for ~60% of the specimen's cross sectional area. SEM results confirm the absence of ASR gel in the interior of this mortar, except within a few millimeters from the surface. This strongly agrees with the presence of an $[OH^-]$ gradient as predicted by the numerical modeling.

To evaluate the contributions of alkali binding versus ion diffusion on $[OH^-]$ profiles, two hypothetical mortars were simulated. The first mortar (shown as diamonds in Fig. 4) had the same ion diffusivity as the 100%PC mortar but had a higher alkali binding capacity similar to the 15%F1 mortar. The second mortar (shown as circles in Fig. 4) had the same alkali binding capacity as the 100%PC mortar but had a lower ion diffusivity similar to the 15%F1 mortar. By comparison, it is evident that the effect of reduced ion diffusivity is more significant than the effect of improved alkali binding in reducing $[OH^-]$. Overall, both mechanisms delay the penetration of NaOH which favors less ASR.

5.5. Tensile and compressive strength

The results of the tensile and compressive strength measurements of the mortars after 3 days submersion in the NaOH bath are shown in Fig. 5. The error bars represent ±1 standard deviation based on measurements of four duplicate samples. The results in Fig. 5 are normalized by dividing by the corresponding strengths of the control (100%PC) mortar. The control mortar had an average tensile strength of 5.55 MPa and compressive strength of 25.2 MPa at this age. Commonly, it is assumed that replacing Portland cement with fly ash results in a reduction in the early-age strength [33]. In the environment of the ASTM C1567 test, however, it is observed that mortars containing fly ash show 15–38% increase in the average tensile strength compared to the 100%PC mixture. Error bars representing ±1 standard deviation are included to show that improvement in the tensile strength of fly ash mortars is statistically significant. Assuming a normal distribution, the probability of any of these fly ash mortars showing a lower tensile strength than the control mortar is only 2.5%.

Such tensile strength improvements could be primarily attributed to the reduced pore size (i.e., flaw size) in the fly ash mortars as discussed before and in [74]. In addition, some level of microcracking may be expected due to ASR at the surface of the control mortar, which reduces the measured tensile strength. Improvement in the compressive strength of the fly ash mortars was in the range 0–54%. The compressive strength is less dependent on the flaw size and the presence of surface flaws.

An increase in the tensile strength of mortars in the ASTM C1567 test has two benefits. First, it prevents or delays the formation of cracks. Cracking provides immediate access of the NaOH solution to the interior of the specimen, which significantly accelerates ASR. Second, by delaying ASR, fly ash provides additional time to allow the hydration of the binder to proceed, which results in a denser and less permeable paste matrix. This can further mitigate alkali transport, formation and swelling of the gel, and cracking. It should be noted that the increase in the early-age tensile strength of fly ash mortars may be an artifact of the ASTM C1567 test which exposes

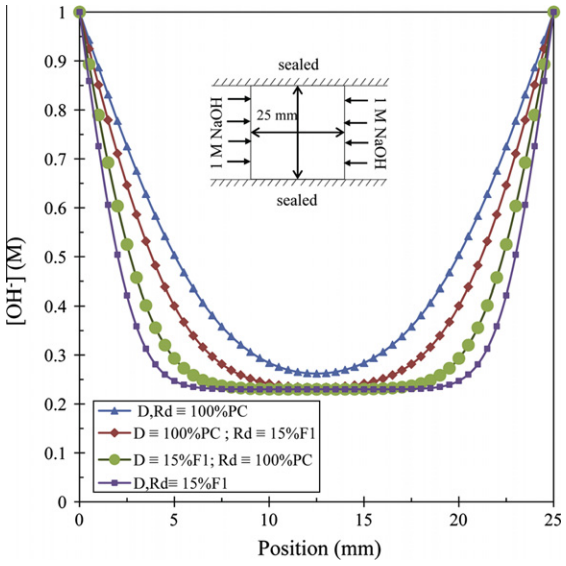

Fig. 4. Simulation results showing the OH^- concentrations at the conclusion of the ASTM C1567 test for different diffusion and binding coefficients.

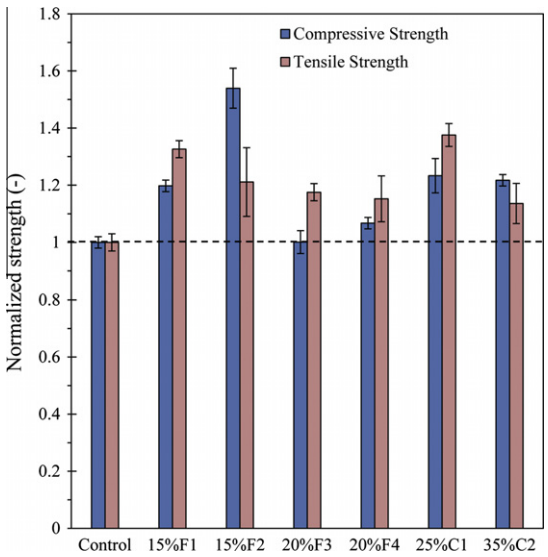

Fig. 5. Normalized (to the control mortar) tensile and compressive strengths of mortars 3 days after exposure to 1 M NaOH solution.

specimens to high temperatures and alkalinities. Such an environment significantly promotes the pozzolanic reactions of fly ash. In real field exposures, the pozzolanic reaction of fly ash may result in higher tensile strengths only after a long term.

5.6. Microstructural analysis (SEM/EDS)

SEM/EDS imaging was performed to answer two main questions. First, does ASR gel form in large quantities in fly ash mortars? Second, does the presence of fly ash alter the composition of ASR gel and as such, change its viscosity and swelling pressure as suggested by [29,38]. Previous research by Bleszynski and Thomas [37] on ASTM C1567 prisms containing reactive flint showed that significant dissolution of aggregates and formation of gel could occur in mortars containing fly ash. However, probably due to its low viscosity, this ASR gel could flow freely through the cement paste matrix without exerting large stresses and cracking.

Fig. 6a and b show SEM images of the 100%PC and 15%F1 mortars at the conclusion of the ASTM C1567 test. The control specimen is severely distressed by ASR throughout the specimen thickness. Other SEM images (not included) reveal that ASR is more severe and larger volumes of gel have formed near the perimeter versus the interior of mortar prisms. This supports the claim that ion transport has an important role during the ASTM C1567 test. The fly ash mortars only contained traces of ASR gel near the exposed surface of the mortar bars. A summary of the EDS compositional analysis of the ASR gel from the control and fly ash mortars is presented in Table 3. The results show that the gel compositions are approximately similar; no appreciable differences in the Ca/Si or Ca/Na between the control and fly ash mortars are observed. This could mean that ASR gel may have comparable compositions in the control versus fly ash mortars. It is the massive volume of gel produced in the control mortar that leads to its deterioration, in comparison with small quantities of gel in fly ash mortars. In addition, it was found that although the volume of gel formed is increasing with time in all mortars, there is only a slight variation in the gel composition based on EDS analysis between 7 and 14 days NaOH exposure. Also variations in the gel composition from the perimeter to the interior of 100%PC mortar prisms were small.

5.7. Aggregate dissolution rate

To evaluate the dissolution rate of glass aggregates and the potential benefits of fly ash, a glass corrosion experiment was performed in which the dissolution (i.e., mass loss) of soda–lime glass slides exposed to a constant volume ($V = 340$ ml) of 1 M NaOH solution was monitored over time. Each corrosion cell contained two glass slides with a total surface area of SA = 79×10^{-4} m^2. Duplicate experiments were performed in the absence of fly ash or by adding 10 g or 20 g of F1 fly ash (specific surface area = 0.2624 m^2/g) to the system. The initial pH = 14.00 was similar in all three cells and increased only slightly during the experiment, to pH = 14.03 for the cell without fly ash and pH = 14.06 for the two cells containing fly ash. This slight increase in the pH is due to dissolution of alkalis from the soda-lime glass, per Eq. (3). The goal of this experiment was to evaluate whether fly ash can reduce silica dissolution even in systems with very similar pore solution alkalinity (pH).

The results are presented in Fig. 7. The rate of mass loss from slides is higher in the system without fly ash. At 14 days, the mass loss of slides was 48% or 62% lower when 10 g or 20 g fly ash was present. This is likely due to a drastic increase in the silicate surface area to solution volume ratio (SA/V) as a result of the silicate area provided by the fly ash (note that fly ash is mainly an aluminosilicate glass that also contains some crystalline silicate phases).

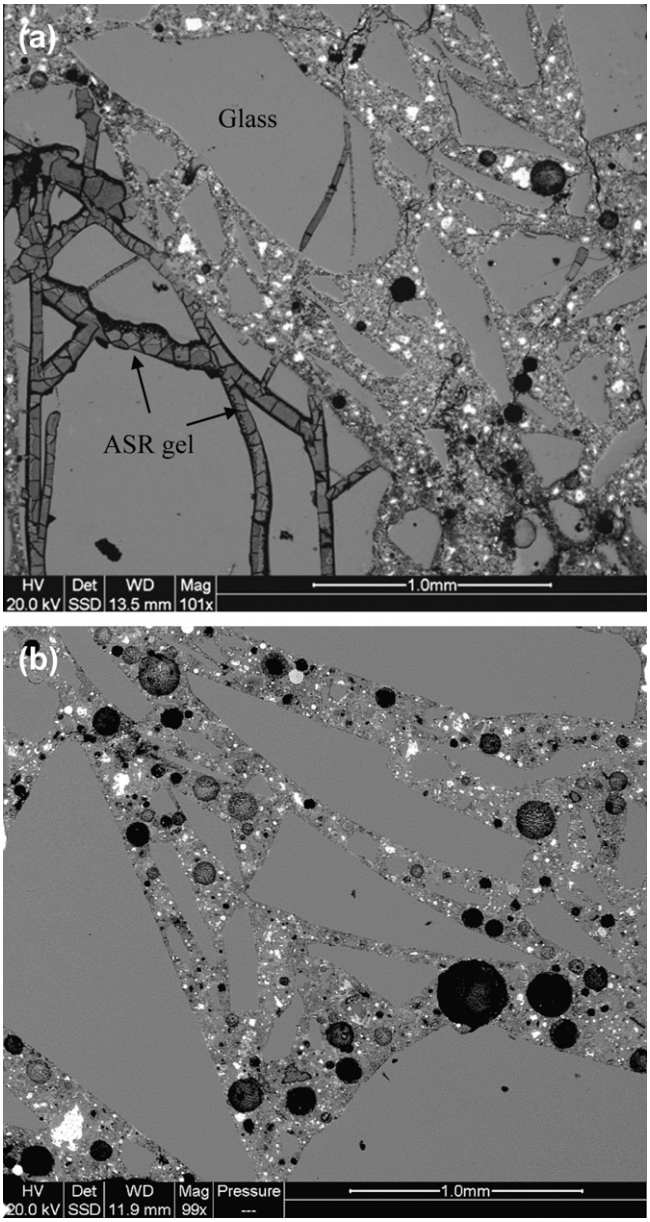

Fig. 6. SEM micrographs of: (a) control mortar and (b) 15%F1 mortar at the conclusion of the ASTM C1567 test.

While the solution volume remained at $V = 340$ ml, the silicate surface area increased to SA = 2.63 m^2 or SA = 5.26 m^2 for 10 g or 20 g fly ash addition, respectively. As a result, the concentration of OH^- ions (which are responsible for dissolving both glass slides and fly ash) decreases significantly per unit silicate surface area. For 340 ml 1 M NaOH solution, the OH^- concentration per unit silicate surface area is 43,038 mM/m^2 when no fly ash is present. This value drops to 129.3 or 64.6 mM/m^2 when 10 g or 20 g F1 fly ash is added, assuming that all the fly ash surface is accessible to the solution.

The results presented in Fig. 7 suggest a new mechanism which could contribute to mitigation of ASR when SCMs are present. By increasing the accessible silicate surface area, the SCM reduces the effective concentration of OH^- at the surface of aggregates; and as such, reduces the aggregate dissolution rate. Even if SCM is incapable of reducing the pH of pore solution (e.g., near the exposed surface of mortar in ASTM C1567 teat), the mere presence of SCM increases the accessible silicate surface area and should reduce the aggregate dissolution rate.

Table 3
Average atomic composition (wt.%) of ASR gel measured by EDS.

		Na	Ca	Si	K	Al	Mg	Ca/Si	Ca/Na
At 7 days	Control	7.76	4.91	24.81	1.29	0.64	0.37	0.2	0.63
	15%F1	9.04	5.33	24.37	1.66	1.56	1.44	0.22	0.59
	35%C2	8.95	5.23	24.49	2.00	1.19	–	0.21	0.58
At 14 days	Control	10.63	6.73	22.39	0.31	0.77	0.36	0.3	0.63
	15%F1	7.24	5.5	24.89	0.64	0.73	0.37	0.22	0.76
	35%C2	9.28	5.86	23.42	1.02	0.65	0.37	0.25	0.63

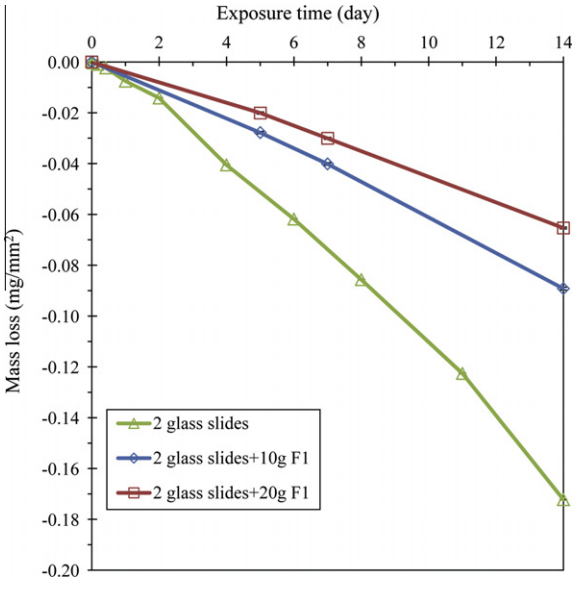

Fig. 7. Mass loss of glass slides in 1 M NaOH solution at 80 °C in the presence or absence of fly ash.

6. Conclusions

The results of this study suggest that fly ash can effectively mitigate ASR during the ASTM C1567 test through the following mechanisms:

- Fly ash reduces the alkalinity ($[OH^-]$) of pore solution by significantly reducing the ion diffusion coefficient of mortars. A diffusivity reduction by a factor of 4–7 was recorded, as early as 48 h after casting, when sufficient dosage of fly ash replaced Portland cement. This diffusivity reduction is partly due to reduction in the porosity and pore size when cement is replaced with a lower density and finer size fly ash, and partly due to the pozzolanic reaction promoted by the high temperature and alkalinity of the system. As a result of the lower ion diffusivity, the external NaOH penetrates slower into fly ash mortars, resulting in a lower pore fluid alkalinity, and significantly slower ASR. The results of SEM imaging, pore fluid analysis, and numerical modeling all confirm the significant role of ion transport during the ASTM C1567 test.
- Fly ash reduces the alkalinity ($[OH^-]$) of pore solution through alkali binding. Fly ash reduces the C/S of C–S–H gel which in turn, improves its alkali binding capacity. In addition, more C–S–H is produced by pozzolanic reactions. As such, a considerable fraction of the penetrated NaOH is removed from the pore solution. The results of the numerical model suggested that the contribution of transport reduction is more significant than the effect of an improved alkali binding.
- Fly ash increases the tensile strength of ASTM C1567 mortars and may prevent or delay the onset of cracking. This also prevents an accelerated transport of NaOH through cracks to the interior of the mortar specimens.
- Fly ash can reduce the dissolution rate of siliceous aggregates even when the pH of pore solution is maintained constant (e.g., near the perimeter of mortar prisms that are exposed to the external NaOH bath). Fly ash provides a large silicate surface area that is accessible to the corrosive OH^- ions. As such, the concentration of OH^- per unit surface area of silicate is markedly reduced. In other words, for a unit volume of pore solution at a given pH, a large fraction of hydroxyl ions are involved in dissolving fly ash instead of attacking the reactive aggregates.

The results of this work also suggest that alkali dilution and modifying ASR gel composition are not major contributors to mitigation of ASR by fly ash during the ASTM C1567 test.

Acknowledgements

The authors gratefully acknowledge support received from the National Science Foundation (NSF) under Grant No. CMMI 1030708 granted to the fourth author. Further support from Hawaii Department of Transportation under Project No. HWY-L-2.6129 is appreciated. Any opinions, findings and conclusions or recommendations expressed in this material are those of the authors and do not necessarily reflect the views of the National Science Foundation or Hawaii Department of Transportation. The authors are very thankful to Dr. Carlo Pantano for his valuable suggestions and contributions.

References

[1] ASTM C1567-11. Standard test method for determining the potential alkali–silica reactivity of combinations of cementitious materials and aggregate (accelerated mortar-bar method). West Conshohocken, Pennsylvania: American Society for Testing and Materials; 2011.
[2] Diamond S. A review of alkali–silica reaction and expansion mechanisms, 2. Reactive aggregates. Cem Concr Res 1976;6:549–60.
[3] Poole AB. Introduction to alkali-aggregate reaction in concrete. In: Swamy RN, editor. The alkali silica reaction in concrete. New York: Van Nostrand Reinhold; 1992.
[4] Hobbs DW. Alkali–silica reaction in concrete. London: Thomas Telford; 1988.
[5] Stanton TE. Expansion of concrete through reaction between cement and aggregate. Proc Am Soc Civil Eng 1940;66(10):1781–811.
[6] Carrasquillo RL, Snow PG. Effect of fly ash on alkali-aggregate reaction in concrete. ACI Mater J 1987;84(4):299–305.
[7] Chen H, Soles JA, Malhotra VM. Investigations of supplementary cementing materials for reducing alkali-aggregate reactions. Cem Concr Compos 1993;15(1–2):75–84.
[8] Duchesne J, Bérubé MA. Long-term effectiveness of supplementary cementing materials against alkali–silica reaction. Cem Concr Res 2001;31(7):1057–63.
[9] Hobbs DW. Deleterious expansion of concrete due to alkali–silica reaction: influence of Pfa and slag. Mag Concr Res 1986;38(137):191–205.
[10] Thomas MDA. The effect of supplementary cementing materials on alkali–silica reaction: a review. Cem Concr Res 2011;41:209–16.
[11] Diamond S. Effects of two Danish fly ashes on alkali contents of pore solutions of cement-fly ash pastes. Cem Concr Res 1981;11(3):383–94.
[12] Dunstan ER. The effect of fly ash on concrete alkali-aggregate reaction. Cem Concr Aggreg 1981;3:101–4.
[13] Hobbs DW. Influence of pulverized-fuel ash and granulated blast furnace slag upon expansion caused by the alkali–silica reaction. Mag Concr Res 1982;34(1):83–94.

[14] Hobbs DW. The effectiveness of fly ash in reducing the risk of cracking due to ASR in concretes containing cristobalite. Mag Concr Res 1994;46(168):167–75.
[15] Nagataki S, Ohga H, Inoue T. Evaluation of fly ash for controlling alkali-aggregate reaction. In: Proc. 2nd Int. Conf. On Durability of Concrete. Montreal, Canada, 1991, p. 955–972.
[16] ASTM C1293-08b. Standard test method for determination of length change of concrete due to alkali–silica reaction. West Conshohocken, Pennsylvania: American Society for Testing and Materials; 2008.
[17] Shayan A, Diggins R, Ivanusec I. Effectiveness of fly ash in preventing deleterious expansion due to alkali-aggregate reaction in normal and steam-cured concrete. Cem Concr Res 1996;26(1):153–64.
[18] Thomas MDA. Field studies of fly ash concrete structures containing reactive aggregates. Mag Concr Res 1996;48(177):265–79.
[19] Thomas MDA, Innis FA. Use of the accelerated mortar bar test for evaluating the efficacy of mineral admixtures for controlling expansion due to alkali–silica reaction. Cem, Concr Aggreg 1999;21(2):157–64.
[20] Berra M, Mangialardi T, Paolini AE. Application of the NaOH bath test method for assessing the effectiveness of mineral admixtures against reaction of alkali with artificial siliceous aggregate. Cem Concr Compos 1994;16(3):207–18.
[21] Ideker JH, Drimalas T, Bentivegna AF, Folliard KJ, Fournier B, Thomas MDA et al. The importance of outdoor exposure site testing. 14th ICAAR, international conference on alkali aggregate reactions. Austin, Texas, 2012.
[22] Thomas MDA, Fournier B, Folliard K, Ideker J, Shehata M. Test methods for evaluating preventive measures for controlling expansion due to alkali–silica reaction in concrete. Cem Concr Res 2006;36(10):1842–56.
[23] Lindgård J, Andiç-Çakır Ö, Fernandes I, Rønning TF, Thomas MDA. Alkali–silica reactions (ASR): literature review on parameters influencing laboratory performance testing. Cem Concr Res 2012;42:223–43.
[24] ASTM C311-07. Standard test method for sampling and testing fly ash or natural pozzolans for use in Portland-cement concrete. West Conshohocken, Pennsylvania: American Society for Testing and Materials; 2007.
[25] Duchesne J, Bérubé MA. The effectiveness of supplementary cementing materials in suppressing expansion due to ASR; II: Pore solution chemistry. Cem Concr Res 1994;24(8):1579–81.
[26] Canham I, Page CL, Nixon PJ. Aspects of the pore solution chemistry of blended cements related to the control of alkali silica reaction. Cem Concr Res 1987;17(5):839–44.
[27] Rayment PL. The effect of pulverised-fuel ash on the c/s molar ratio and alkali content of calcium silicate hydrates in cement. Cem Concr Res 1982;12(2):133–40.
[28] Hong SY, Glasser FP. Alkali binding in cement pastes: Part I. The C–S–H phase. Cem Concr Res 1999;29(12):1893–903.
[29] Monteiro PJM, Wang K, Sposito G, dos Santos MC, de Andrade WP. Influence of mineral admixtures on the alkali-aggregate reaction. Cem Concr Res 1997;27(12):1899–909.
[30] Shehata MH, Thomas MDA. The effect of fly ash composition on the expansion of concrete due to alkali–silica reaction. Cem Concr Res 2000;30(7):1063–72.
[31] Shehata MH, Thomas MDA. Alkali release characteristics of blended cements. Cem Concr Res 2006;36(6):1166–75.
[32] Lothenbach B, Scrivener K, Hooton RD. Supplementary cementitious materials. Cem Concr Res 2011;41:217–29.
[33] Pandey SP, Sharma RL. The influence of mineral additives on the strength and porosity of OPC mortar. Cem Concr Res 2000;30(1):19–23.
[34] Li Y, Chen Y, Wei J, He X, Zhang H, Zhang W. A study on the relationship between porosity of the cement paste with mineral additives and compressive strength of mortar based on this paste. Cem Concr Res 2006;36(9):1740–3.
[35] Mindess S, Young JF, Darwin D. Concrete. 2nd ed. Upper Saddle River, New Jersey: Prentice Hall; 2002.
[36] Struble LJ, Diamond S. Swelling properties of synthetic alkali silica gels. J Am Ceram Soc 1981;64(11):652–5.
[37] Bleszynski RF, Thomas MDA. Microstructural studies of alkali–silica reaction in fly ash concrete immersed in alkaline solutions. Adv Cem Based Mater 1998;7(2):66–78.
[38] Bonakdar A, Mobasher B, Dey SK, Roy DM. Correlation of reaction products and expansion potential in alkali–silica reaction for blended cement materials. ACI Mater J 2010;107(4):380–6.
[39] Chatterji S. The role of $Ca(OH)_2$ in the breakdown of Portland cement concrete due to alkali–silica reaction. Cem Concr Res 1979;9(2):185–8.
[40] Hobbs DW. Alkali–silica reaction in concrete. In: Bensted J, Barnes P, editors. Structure and performance of cements. London: Spon Press; 2002.
[41] Moser RD, Jayapalan AR, Garas VY, Kurtis KE. Assessment of binary and ternary blends of metakaolin and class C fly ash for alkali–silica reaction mitigation in concrete. Cem Concr Res 2010;40:1664–72.
[42] Rajabipour F, Sant G, Weiss J. Interactions between shrinkage reducing admixtures (SRAs) and cement paste's pore solution. Cem Concr Res 2008;38(5):606–15.
[43] Warner SJ. The role of alumina in the mitigation of alkali–silica reaction. M.S. thesis. Corvallis, Oregon: Oregon State University; 2012.
[44] Aquino W, Lange DA, Olek J. The influence of metakaolin and silica fume on the chemistry of alkali–silica reaction products. Cem Concr Compos 2001;23:485–93.
[45] Hong SY, Glasser FP. Alkali sorption by C–S–H and C–A–S–H gels: Part II. Role of alumina. Cem Concr Res 2002;32(7):1101–11.
[46] Chappex T, Scrivener K. Alkali fixation of C–S–H in blended cement pastes and its relation to alkali silica reaction. Cem Concr Res, in press. doi: 10.1016 (2012).
[47] Iler RK. The chemistry of silica: solubility, polymerization, colloid and surface properties, and biochemistry. New York: Wiley; 1979.
[48] Bickmore BR, Nagy KL, Gray AK, Brinkerhoff AR. The effect of $Al(OH)_4^-$ on the dissolution rate of quartz. Geochim Cosmochim Acta 2006;70:290–305.
[49] Chappex T, Scrivener K. Controlling alkali–silica reaction by understanding the contribution of aluminum provided by supplementary cementitious materials. 14th ICAAR, international conference on alkali aggregate reactions, Austin, TX, 2012.
[50] Sang JC, Jakubic RF, Barkatt A, Saad EE. The interaction of solutes with silicate glass and its effect on dissolution rates. J Non-Cryst Solids 1994;167:158–71.
[51] Rajabipour F, Maraghechi H, Fischer G. Investigating the alkali–silica reaction of recycled glass aggregates in concrete materials. ASCE J Mater Civil Eng 2010;22(12):1201–8.
[52] ASTM C1260-07. Standard test method for potential alkali reactivity of aggregates (mortar-bar method). West Conshohocken, Pennsylvania: American Society for Testing and Materials; 2007.
[53] Maraghechi H, Shafaatian SMH, Fischer G, Rajabipour F. The role of residual cracks on alkali silica reactivity of recycled glass aggregates. Cem Concr Compos 2012;34:41–7.
[54] Rajabipour F, Maraghechi H, Shafaatian S. ASR and its mitigation in mortars containing recycled soda-lime glass aggregates. 14th ICAAR, international conference on alkali aggregate reactions, Austin, Texas, 2012.
[55] Hou X, Struble LJ, Kirkpatrick RJ. Formation of ASR gel and the role of C–S–H and portlandite. Cem Concr Res 2004;34:1683–96.
[56] ASTM C150/C150M-11. Standard specification for Portland cement. West Conshohocken, Pennsylvania: American Society for Testing and Materials; 2011.
[57] ASTM C618-08a. Standard specification for coal fly ash and raw or calcined natural pozzolan for use in concrete. West Conshohocken, Pennsylvania: American Society for Testing and Materials; 2008.
[58] ASTM C305-06. Standard practice for mechanical mixing of hydraulic cement pastes and mortars of plastic consistency. West Conshohocken, Pennsylvania: American Society for Testing and Materials; 2006.
[59] Garboczi EJ. Permeability, diffusivity, and microstructural parameters: a critical review. Cem Concr Res 1990;20(4):591–601.
[60] Christensen BJ, Coverdale T, Olson RA, Ford SJ, Garboczi EJ, Jennings HM, et al. Impedance spectroscopy of hydrating cement-based materials: measurement, interpretation, and application. J Am Ceram Soc 1994;77(1):2789–804.
[61] Akhavan A, Rajabipour F. Evaluating ion diffusivity of cracked cement paste using electrical impedance spectroscopy, Mater Struct, in press: doi: 10.1617/s11527-012-9927-x.
[62] Rajabipour F. Insitu electrical sensing and material health monitoring in concrete structures. Ph.D. dissertation. Purdue University, West Lafayette, Indiana, December 2006, 193pp.
[63] CRC Handbook of chemistry and physics. 90th ed. Boca Raton, Florida: CRC Press; 2010.
[64] Scrivener KL, Füllmann T, Gallucci E, Walenta G, Bermejo E. Quantitative study of Portland cement hydration by X-ray diffraction/Rietveld analysis and independent methods. Cem Concr Res 2004;34:1541–7.
[65] Olson RA, Jennings HM. Estimation of C–S–H content in a blended cement paste using water adsorption. Cem Concr Res 2001;31:351–6.
[66] Malvar LJ, Lenke LR. Efficiency of fly ash in mitigating alkali–silica reaction based on chemical composition. ACI Mater J 2006;103(5):319–26.
[67] Clark DE, Yen-Bower EL. Corrosion of glass surfaces. Surf Sci 1980;100:53–70.
[68] Gartner EM, Young JF, Damidot DA, Jawed I. Hydration of Portland cement. In: Bensted J, Barnes P, editors. Structure and performance of cements. London: Spon Press; 2002.
[69] Thomas NL, Double DD. Calcium and silicon concentrations in solution during the early hydration of Portland cement and tricalcium silicate. Cem Concr Res 1981;11(5–6):675–87.
[70] Taylor HFW. Cement chemistry. New York: Academic Press; 1990.
[71] Lothenbach B, Winnefeld F. Thermodynamic modeling of the hydration of Portland cement. Cem Concr Res 2006;36:209–26.
[72] Stumm W, Morgan JJ. Aquatic chemistry: chemical equilibria and rates in natural waters. New York: Wiley-Interscience; 1995.
[73] Shimada Y, Young JF. Thermal stability of ettringite in alkaline solutions at 80 °C. Cem Concr Res 2004;34:2261–8.
[74] Shafaatian SMH. Innovative methods to mitigate alkali–silica reaction in concrete materials containing recycled glass aggregates. Ph.D. dissertation. University Park, Pennsylvania: Pennsylvania State University; 2012.